

Optical Properties of BN in the cubic and in the layered hexagonal phases

Giancarlo Cappellini and Guido Satta

*INFN Sezione di Cagliari and Dipartimento di Fisica, Università di Cagliari, Cittadella
Universitaria, Strada Prov.le Monserrato-Sestu Km 0.700, I-09042 Monserrato (Ca), Italy*

Maurizia Palummo and Giovanni Onida

*INFN Sezione di Roma-2 and Dipartimento di Fisica, Università di Tor Vergata, via della
Ricerca Scientifica 1, I-00133, Rome, Italy*

Abstract

Linear optical functions of cubic and hexagonal BN have been studied within first principles DFT-LDA theory. Calculated energy-loss functions compare well with experiments and previous theoretical results both for h-BN and for c-BN. Discrepancies arise between theoretical results and experiments in the imaginary part of the dielectric function for c-BN. Possible explanation to this mismatch are proposed and evaluated; lattice constant variations, h-BN contamination in c-BN samples and self-energy effects.

Pacs numbers: 78.20 -e, 78.20.Ci, 78.20.Dj, 71.45.Gm

I. INTRODUCTION

The properties of boron nitride (BN) have motivated detailed theoretical and experimental studies since a long time [1,2,3]. Many advanced technologies rely on Boron Nitride and on materials based on it, due the wide spectrum of properties offered by its polymorphic modifications, two graphite-like and two dense ones. Boron nitride shares many of its properties, structures, processings and applications with carbon. Cubic boron nitride (also known as sphalerite boron nitride and abbreviated as Z-BN, c-BN or β -BN), with sp^3 -hybridized B-N bonds, has the diamond crystal structures and a similar lattice constants. Its physical properties, such as extreme hardness, wide energy bandgap, low dielectric constant and high thermal conductivity, are also very near to those of diamond. These amazing properties of c-BN have many appealing applications in modern microeletronic devices, and make it useful also as a protective coating material or in high-duty tools [4]. Hexagonal BN (h-BN or α -BN), an sp^2 -bounded layered compound and graphite also resemble each other in term of crystal structures, lattice constants, and physical properties such as strong anisotropy. Due to its high termal stability h-BN is a widely used material in vacuum technology. It has been employed in microelectronic devices [5], for x-ray lithography masks [6], and as a wear-resistant lubricant [7]. The hexagonal phase is also the underlying structure of the BN nanotubes, which are systems of growing interest nowadays [8,9,10].

On the other hand, significant differences exist between carbon and boron nitride, due mainly to differences in their chemical bonding. Infact h-BN and c-BN mechanical strengths, thermal conductivities and Debye temperatures are lower than in their carbon counterparts. Moreover h-BN is electrically an insulator, while graphite is a conductive semi-metal. In contrast to diamond, which can be readily doped only as a p-type, c-BN can be doped either n- or p-type. Moreover c-BN does not react with ferrous materials, even at high temperatures ($T \sim 1600K$) [11], and, last but not least, both c- and h-BN are more resistent to oxidation than their carbon counterparts [4].

An important issue is the experimental evidences for negative electron affinity (NEA) in

cubic boron nitride samples [12,13]. The electron affinity of a semiconductor is the difference between the vacuum energy level and the conduction band minimum level. NEA occurs when the conduction band minimum lies above the vacuum energy level. Any electron promoted into the conduction band has then enough energy to escape into vacuum. One of the most striking application is in electron emission devices, to obtain the highest electron emission density at the least energy expenditure (cold cathode emitters) [14]. Correct evaluation of the one electron transition energies and the position of the single particle states turn out to be fundamental points relatively to this issue, and will be here addressed in detail.

It is now generally agreed experimentally that bulk c-BN is the thermodynamically stable phase at ambient conditions, and that the less dense h-BN becomes stable at temperatures exceeding $T \sim 1200K$ [15]. Due to the large change in volume, fragmentation and disordering between the two phases can develop. In combination with a rigid lattice, this lead to a large hysteresis of phase transitions. This means that phases created under high pressure high-temperature conditions can persist inside the sample under standard condition [15]. Two other phases, the rhombohedral(r-BN) and the wurtzite (w-BN) are stable only at very high pressure ($P \simeq 10GPa$) [16] and will not be considered here. Structural and excitation properties of wurtzite structure has been studied elsewhere [25]. At ambient pressures an interplay between h-BN and c-BN domains only should be expected [17,18]. Since 1979 c-BN chemical vapor deposited films have been realized [19], but the production of pure c-BN thin films (either by chemical or physical vapor deposition) remains a difficult task due to the formation, during the growth process, of unwilled h-BN domains [18].

Extensive theoretical studies have been performed on the ground-state properties of BN. All calculations founded on density functional theory (DFT) and on the local density approximation (LDA) for the exchange-correlation potential agree in predicting that the c-BN structure has a lower energy than h-BN by about 0.06eV per atom [20,21,22,23]. This result, which is confirmed by our calculation, disagrees with an older calculation based on the orthogonal linear combination of atomic orbitals (OLCAO), where h-BN was found to be more stable than c-BN by 0.35 eV per atom [24]. This is probably explained by a lack of

convergence in the older calculations. Also the band structure properties of BN have been the subject of extensive theoretical work, performed within different schemes and approximations [1,2,8,9,10,20,21,22,23,24,25,26,27,28,29,30,31,32,33,34,35,36,37]. On the experimental point of view many methods have been employed to explore the electronic structure. Among them there are methods like soft-x-ray emission spectroscopy (SXRES) [38,39] and photoelectron spectroscopy(PES) [40], which are both sensitive to occupied states, as well as near-edge x-ray absorption fine structure spectroscopy(NEXAFS) [41,42] and energy loss near edge spectroscopy, which can be used to probe the empty bands(ELNES) [43]. In addition, electron energy loss spectroscopy performed in the plasmon region has proved to provide valuable information [43,44,47].

The experimental optical functions of BN compounds are not as well known as those of the other group III nitrides. This is due in large part to the lack of high quality, single crystal samples. Consequently, most optical studies on BN have been performed on polycrystalline samples, with various amount of impurities. As one could expect, the results of optical studies performed on these materials vary greatly [45,46]. However a general consensus from the experimental data is that the minimum band gap is direct in the case of h-BN, and indirect in the case of c-BN. For h-BN a direct band gap of $5.2 \pm 0.2\text{eV}$ associated to the transition $H_{3v}-H_{2c}$ has been estimated [48], while a value of $6.4 \pm 0.5\text{eV}$ for the indirect minimum band gap in c-BN has been determined [49], and associated to the $\Gamma_{15v}-X_{1c}$ transition [25,33].

In the present paper we present *ab-initio* linear optical functions of c- and h-BN studied within DFT-LDA theory. No external parameter has been used to fit the experimental curves. Due to the importance of the two BN phases, and to the fact that in several experimental configurations they appear together in the same sample, a parallel study of both phases has been accomplished throughout the present paper. Complex dielectric functions, refractive index, reflectance spectra, optical conductivity, and energy loss functions for c-BN and h-BN have been calculated. We report our results in the energy range of interest to compare them with the existing theoretical and experimental literature. Calculated DFT-

LDA energy-loss functions agree with experiments and with previous theoretical results, both for h-BN and c-BN. On the other hand, discrepancies arise between theoretical results and experiments in the imaginary part of the dielectric function for c-BN. Possible explanations of this issue are proposed and evaluated in detail. The imaginary part of the dielectric function in the h-BN case, instead, shows a reasonable agreement with both other theoretical results and experiments.

This paper is organized as follows. In Section II we give the computational details of the calculation of the ground state properties for both phases. In Section III we describe the theoretical scheme used to evaluate the optical properties, and the part related to the calculation of excitation properties. In Sections IV and V we present results for the optical properties of c-BN and h-BN respectively. Finally, in Section VI conclusions are drawn, and the perspectives and issues opened by our work have been presented.

II. COMPUTATIONAL DETAILS AND GROUND STATE CALCULATIONS

Density functional calculations have been carried out within the local density approximation (LDA) for the exchange and correlation functional [50], using the Perdew and Zunger parametrization [52] of the Ceperley and Alder results [51]. Kohn–Sham orbitals are expanded in a plane–wave basis set, with an energy cutoff of 55 *Ry*.

Care has been used in constructing the ionic pseudopotentials, in order to avoid the occurrence of ghost states and to assure an optimal transferability [53,54]. Angular components up to $l = 2$ have been included. Separable, norm–conserving soft pseudopotentials have been generated within the scheme of Martins and Troullier [55], with the following core radii (bohr): 1.59 (B, 3*d*), 1.49 (N, 2*p*). For Boron, non linear core corrections (NLCC) to be used in the solid calculation, have been taken into account in generating pseudopotentials and pseudowavefunctions [56].

With the selected plane-waves cutoff, both the total energy and Kohn-Sham eigenvalues are converged to better than 0.1 eV for both c-BN and h-BN. For the cubic phase, the use of

10 special Chadi and Choen k points for charge integration in the first Brillouin Zone (BZ) [57], is found to be sufficient to achieve a good accuracy for the computed total energy; for instance, total energy changes by less than 10 meV, and the fundamental band gap by less than 0.1 eV, when passing from 6 to 10 special points for BZ sampling. For the layered hexagonal case the use of 12 k points are sufficient for a full convergency of the total energy and eigenvalues.

Hexagonal BN, turns out to be less stable than the cubic BN by about 0.050 eV/atom. Preliminary calculations in which "hard" norm-conserving pseudopotentials of the Bachelet, Hamann, Schlüter (BHS) form were used with energy cutoff of 150 Rydberg [25] gave an energy difference of 0.078 eV/atom. Our results hence confirm the previous finding that c-BN is more stable than h-BN. No contributions to the total energy coming from zero point vibration of the lattices have been considered [18,20].

In Table(I) the structural parameters for the two phases are reported, in comparison with previous theoretical calculations and experiments. For c-BN our equilibrium lattice parameter underestimates the experimental one by few percent as usual for DFT-LDA, in accordance with previous theoretical results. The bulk modulus falls very near to the experimental energy range [20,24].

An underestimation of the same order is found for the two lattice parameters a and $\frac{c}{a}$ of h-BN, as reported by other authors too [20,24].

No large differences in equilibrium structural parameters arise when the harder BHS pseudopotentials and the larger cutoff are used [25].

III. OPTICAL PROPERTIES AND ELECTRONIC EXCITATIONS

The experimental scenario about the electronic properties of Boron Nitride is characterized by many measurements. For h-BN, however, several old optical and energy loss data have been very conflicting each other mostly because of the use of poor samples. Band structures calculated in the past were not accurate enough to be of real help [24]. Recently,

careful measurements of inelastic-electron-scattering spectra on well characterized h-BN became available [47], and accurate measurements of the linear optical properties of c-BN have been reported [45]. Ellipsometry measurements have also been done to characterize noncrystalline thin films of BN [47,58], and optical reflectance spectra of c-BN have been recently published [46].

We determine the optical properties of h-BN and c-BN by calculating the momentum matrix elements (MME) associated with dipole transitions at a large number of k-points in the BZ. The frequency-dependent imaginary part of the dielectric function is given by [59,60]

$$\epsilon''_{\alpha\alpha}(\omega) = \frac{(8\pi)^2 e^2}{\omega^2 m^2 V} \sum_{v,c} \sum_{\vec{k}} | \langle v, \vec{k} | p_{\alpha\alpha} | c, \vec{k} \rangle |^2 \delta(E_c(\vec{k}) - E_v(\vec{k}) - \hbar\omega) \quad (1)$$

where v and c label the valence and conduction states associated with the energies $E_v(\vec{k})$, $E_c(\vec{k})$, V is the crystal volume, and $\langle \rangle$ is the matrix element of the momentum operator. Nonlocality effects in the ionic pseudopotentials are neglected in the evaluation of ϵ_2 [59]. Eigenvalues and eigenfunctions appearing in Eq.(1), are those determined within the DFT-LDA scheme. As it appears from Eq.(1), local field effects are also neglected in the dielectric function calculation [59]. Reference formulas for the macroscopic optical functions, namely [61]

$$N(\omega) = n(\omega) + ik(\omega) \quad (2)$$

for the complex refraction index, will be frequently used in the following. Its relation with the complex macroscopic dielectric function reads:

$$N^2(\omega) = \epsilon(\omega) \quad (3)$$

with

$$\epsilon_1(\omega) = n^2(\omega) - k^2(\omega) \quad (4)$$

and

$$\epsilon_2(\omega) = 2n(\omega)k(\omega) . \quad (5)$$

The absorption coefficient reads (c is the speed of light)

$$\eta(\omega) = 2\omega k(\omega)/c \quad (6)$$

which can be directly connected with the imaginary part of the dielectric function

$$\eta(\omega) = \omega\epsilon_2(\omega)/n(\omega)c \quad (7)$$

and to the optical conductivity σ

$$\sigma(\omega) = \eta(\omega)n(\omega)c/4\pi \quad (8)$$

In the above formulas once ϵ_2 (or $k(\omega)$) is calculated or measured, the correspondent real part ϵ_1 (or $n(\omega)$) can be determined via the Kramers-Kroenig transformation [61].

To give an overview of the optical properties of the two crystals, and in particular of the differences among the hexagonal and the cubic phase, the calculated interband optical conductivity σ is reported in in Fig. 1 and in Fig. 2. In the case of h-BN, an average over the three crystallographic directions is taken. The Joint Density of States (JDOS) for the same samples are also shown. Both the absorption threshold and the oscillator strengths in h-BN are much smaller than in c-BN. In the two cases, our data fairly reproduce the orthogonalized LCAO ones by Xu and Ching [24]. In both crystals there is a very little resemblance between the optical conductivity and the JDOS curves, especially in the high frequency region, indicating a strong \vec{k} dependence of the MME. Both phases show a fundamental indirect band gap, but in h-BN the indirect gap is smaller than in c-BN [9,25,33]. This leads to the lower absorption threshold in h-BN. Many structures can be directly related to measured ones, like the peak around 6 eV for h-BN which can be assigned to transition between bands in the in-plane directions. This correspondence reflects the strong anisotropy in the optical absorption of this material, which shows up even when macroscopic quantities are taken into account (Eq.(2)-Eq.(8)).

As is well known DFT-LDA band structures for semiconductors and insulators cannot reproduce the real (experimental) ones. DFT-LDA eigenvalues, when interpreted as quasiparticle (QP) energies show the so called *band gap problem* [62]. The QP energies correspond only qualitatively to the DFT-LDA ones, mainly because the band gaps between conduction and valence bands show a systematic underestimation with respect to the experiments [63,64,65]. This problem can be solved, for semiconductors and insulators, within a self-energy scheme, called GW [66]. Within this method, the self-energy operator reads $\Sigma = GW$, where G is the one-electron Green function and W the screened Coulomb interaction in the system, fully taking into account the screening properties of the material [62,66,67]. The corresponding Dyson equation can be solved within first-order perturbation theory with respect to $(\Sigma - V_{xc})$, where V_{xc} is the DFT-LDA exchange and correlation potential. Assuming the DFT-LDA eigenvalues and eigenfunctions as the zeroth order eigenvalues and eigenfunctions of the system respectively, the QP corrections for the Bloch state $\psi_{n\vec{k}}$ state read [62]:

$$E_{n\vec{k}} - E_{n\vec{k}}^{(0)} = \frac{\Sigma_{n\vec{k}}^{\text{coh}}(E_{n\vec{k}}^{(0)}) + \Sigma_{n\vec{k}}^{\text{sex}}(E_{n\vec{k}}^{(0)}) - \langle \psi_{n\vec{k}} | V_{xc} | \psi_{n\vec{k}} \rangle}{1 + d\Sigma_{n\vec{k}}(E)/dE|_{E_{n\vec{k}}^{(0)}}} \quad (9)$$

where $\Sigma_{n\vec{k}}^{\text{coh}}$, $\Sigma_{n\vec{k}}^{\text{sex}}$ and $V_{xc,n\vec{k}}^{LDA}$ are the expectation values of the Coulomb Hole (COH), Screened Exchange (SEX) contributions to the self energy, and of the DFT-LDA exchange-correlation (XC) potential, respectively. [62] *Ab-initio* GW schemes are based on the full calculation of the screening function of the system (i.e. fully including local field and dynamical effects) starting from DFT-LDA eigenvalues and eigenfunctions. These kind of calculations for semiconductors and insulators have often led to a very good agreement between theory and experiment [62,67].

Self-energy corrections to the DFT-LDA band structure for semiconductors and insulators can also be performed, with very good results, also using a model dielectric function to mimic the real screening of the system [63,64,65]. One can start for a perturbative formula of the form: [68]

$$E_{n\vec{k}} - E_{n\vec{k}}^{(0)} = \frac{\Sigma_{n\vec{k}}^{\text{coh}} + \Sigma_{n\vec{k}}^{\text{sex}} + \Sigma_{n\vec{k}}^{\text{dyn}}(E_{n\vec{k}}^{(0)}) - \langle \psi_{n\vec{k}} | V_{\text{xc}} | \psi_{n\vec{k}} \rangle}{1 + d\Sigma_{n\vec{k}}(E)/dE|_{E_{n\vec{k}}^{(0)}}} \quad (10)$$

where $\Sigma_{n\vec{k}}^{\text{dyn}}(E_{n\vec{k}}^{(0)})$ is the zeroth order term of the energy expansion of the dynamical part of Σ , and only the static parts of the SEX and COH self-energy are present [62,68]. Corrections to the DFT-LDA spectra calculated from Eq.(10) with the use of model dielectric functions enabled both us and other authors to obtain very positive results, when compared with experiments and *ab-initio* GW ones, in several semiconductors and insulators [69,84]. Moreover, the use of model screening functions enables one to perform GW calculation in a more efficient way, reducing the computational effort of at least one order of magnitude in CPU time [68,84]. Details concerning the evaluation of the different coefficient appearing in Eq.(10) and how do they compare with the *ab-initio* calculated ones are given elsewhere [69,85].

Either *ab-initio* or simplified GW schemes have been employed to calculate the QP energies of h-BN and c-BN [25,33,37,70]. All theoretical results improve the agreement with experimental data. Typically, LDA transition energies suffer of an underestimation of about 3eV for the cubic phase, and 2eV for the hexagonal one [25]. In Tab.(II) and Tab.(III) for c-BN and h-BN respectively we report the results of previous calculations and experiments, namely the fundamental gaps and the main transition energies, in comparison with present results. In c-BN the present transition energies have been calculated at the corresponding theoretical lattice constant while in ref. [33], (as explicitly stated by the authors) the experimental lattice parameter has been used. Moreover, the use of an efficient method in a large gap system induces a slight overestimation of the above energies [25,85]. As it is clear from the data, minor differences arise between the *ab-initio* GW results and the efficient GW ones.

In Tab.(III), the value marked with "a" correspond to a transition between a point T_1 (along the $\Gamma - K$ direction near K, and near in energy to H_v) and M_c . Similarly the term with "b" is the transition energy between $K_{3v}-K_{3c}$, which is near in energy to the transition $H_{3v}-H_{2c}$ [33].

IV. CUBIC BN

In Fig. 3 we report the calculated dielectric function for c-BN obtained within DFT-LDA. The static dielectric constant is found to be of 5.45, larger than the experimental one (4.45) [71]. This fact must be ascribed to absence of local fields effects in the calculation of ϵ_2 [36,60]. Experimental curves obtained from recent optical reflectance measurements in the energy range 5 ÷ 25 eV with synchrotron radiation by Osaka e coworkers [46] are also reported. Two different samples have been used by them, namely a sintered c-BN plate and c-BN thin film. The c-BN sintered plate produced at high pressure and temperature, offered by Sumimoto Electric Industry (Japan), had dimension of 5x5x0.5mm³ and was characterized as cubic by using X-ray diffraction and Raman Scattering [46]. The film, on the other hand, was grown using chemical vapor deposition (CVD) on a silicon substrate, with negative self-bias. c-BN phase, syntesized from B_2H_6 (Ar diluition) and N_2 gas mixtures, had a the grain size is 100-200 Å, controlled by Transmission Electron Microscopy (TEM) images.

In Fig. 4 the calculated reflectivity of c-BN is displayed together with the experimental data taken from ref. [46]. Both the spectra show peaks at 11.7 and 14.0eV and a broad structure around 18eV. The authors of ref. [46] claim that the first two peaks correspond to the E1 and E2 peaks of the zinc-blende-type semiconductors [71]. Our theoretical curve shows two structures centered at 12.8 eV and 14.4 eV but no evidence of higher energy peaks results. To enter in further detail with other theoretical data and experiments, we report in Fig. 5 the imaginary part of ϵ_2 , in comparison with two experimental curves by Osaka et al. [46] One of these curves has been obtained from a crystalline sample, and the other from a film grown by CVD technique. In Fig. 6 we also compare our curve with that calculated by Xu and Ching [24], and with a LMTO one calculated at our theoretical lattice parameter [72]. It is significant to discuss these figures in detail. The experimental data show major structures A and B at 9.05 and 11.7 eV, and shoulders at 13.2eV, 16.7eV (C and D) for the crystalline sample. In the ϵ_2 in the c-BN film, the peak A and the shoulders C and D are not present. The spectrum of the c-BN thin film deposited by plasma CVD is similar to that

of the c-BN synthesized under high pressure and temperature. The authors claim that the differences within their spectra is a demonstration of the fact that the microcrystalline c-BN does not grow epitaxially on silicon substrate, and presents a rough surface. They do not mention the value of the absorption onset, but a value of 6.8 eV can be deduced from their figure of ϵ_2 . To consider the correspondence with the electronic transitions, peak A has been associated to the transition $\Gamma_{15v} - \Gamma_{15c}$, the transition $X_{5v}-X_{3c}$ and $X_{5v}-X_{1c}$, peak C to the transition $L_{3v}-L_{3c}$, and peak D at 16.7 eV to $L_{1v}-L_{1c}$ [46]. The present DFT-LDA reflectance spectrum reproduced qualitatively well the experimental curves, but the first peak is found at 12.8eV and the following at 15.2 eV. Fig. 6 also demonstrates that our results do agree with other theoretical calculations (moreover the theoretical curves reported show no remarkable difference in the range 25 – 40 eV which has not been showed in this figure). However, the absorption onset obtained within DFT-LDA is at 8.9 eV, i.e. much *higher* than the experimental one. This issue turns out to be rather singular in sight to the fact that usually, due to the above mentioned *band gap problem*, the DFT-LDA calculated absorption onset should fall at *lower* energies than the experimental ones [35,36,24,62]. In our case the LDA theoretical curve is blueshifted by more than 2eV with respect to the experiment. A similar overestimate is found also by other theoretical calculations [24,36,35]. The interpretation of Christensen and Gorczyca [35] for ϵ_2 is different (away from threshold) from that proposed by Osaka e coworkers [46], Xu and Ching [24] and from our interpretation. Infact the authors of ref. [35] associate the A peak to the transition 3 to 5 at the $1/2\Gamma U$ point, the major peak B to the 4-5 transition along Σ and L point, the C peak to the 4-6 transitions at L, and the D peak to transition 4-6 at Δ and at Σ' . The onset is ascribed to direct transition at Γ . Xu and Ching found A, B and D structures respectively at 10.7eV, 12.6eV and 15.6 eV, but no evidence for the C shoulder in their curve results [24]. Also their data show a rigid blueshift with respect to the experimental curve by about 1.7eV. Our results resemble those of Xu and Ching. Please notice that their name assignments for the spectrum does not match the present ones. Our onset is found at 9.05eV, while the structures A, B, C and D are found respectively at 9.7 eV, 12.5 eV, 14.9 eV, with small

evidence of peak D. Our assignment to band transitions within DFT-LDA agrees with that proposed in Ref. [46], which has also been confirmed by Tsay and coworkers [27].

As far as we know the only other existing experimental data for the minimal direct gap of c-BN are those by Philipps and Taft [3], which yield a value of 14.5 eV. They studied diamond in the vacuum ultraviolet, and they reported data about a c-BN sample displaying structures around 9 and 10 eV, and a peak near 14.5 eV [3]. The BN data were reported as marginal ones by the authors, to support the evidence for a larger direct band gap in c-BN than in diamond. Their value of 14.5eV has been considered as the experimental direct band gap of this material by other authors in the literature [33,71]. On the other hand, these data could be interpreted in good agreement with our DFT-LDA spectra. Infact, one could consider the first structure as the display of the onset (at 9eV in our DFT-LDA calculation) and the major peak as the maximum (at 12.5 eV in our DFT-LDA calculation) (see Fig.s(2)-(4)).

Let us now address in detail the main mismatch between theoretical results (including ours) and the experiments, concerning the onset. One of the points to be considered is the problem of the correct value of the lattice parameter to be used in optical properties calculations. This issue has been raised for BN by experimental and theoretical works [46,36]. In Fig.(7) we reported different DFT-LDA curves for ϵ_2 calculated at different lattice parameters around the equilibrium one. It is evident that the onset of the theoretical absorption meets the experimental one only when the lattice constant is expanded, with respect to the equilibrium one, by 5%. This value appear to be too large, both with respect to the experimental one, and in sight of the fact that: I) usually the DFT-LDA understimation of the lattice constant is about (1%) [73,98], and II) usually the DFT-LDA *underestimates* the absorption onset.

Another possibility is that the sample under experimental study has not been carefully characterized, namely concerning different possibilities of disturbances, as thermal ones, or the presence of (oxide) overlayers [36,46], which we will not address here but which cannot be excluded in principle. In the following, we consider instead the possibility of h-BN

contamination within the c-BN sample. This is possible due to the fact that in normal conditions h-BN domains may be found in c-BN samples [74].

In Fig. 8 and Fig. 9 we also report the real and imaginary part of the refractive index, $N(\omega)$ and the reflectance spectrum in comparison with the experimental data of Miyata and coworkers [45]. The experimental data have been obtained from reflectance measurements over a photon energy range between $2 \div 23\text{eV}$, and from transmittance data in the range $2 \div 7\text{eV}$. A single crystal of c-BN (5mm^2 area x 0.16mm thick) has been used. Both the onset of the absorption coefficient, or the imaginary part of the refractive index, indicate a gap of $6.1 \pm 0.5\text{eV}$. Our results are only in qualitative agreement with these measurements.

We can argue that part of the error comes from the normalization imposed to the experimental curves. Infact, the absolute value of reflectance and transmittance have been obtained by the authors of ref. [45] by imposing that refractive index at $\omega = 2.10\text{ eV}$ equal to 2.117, the value determined by an independent experiment by Gielisser et al. [87]. Within the present work instead, no adjustable parameter has been used to fit the experimental data.

In Fig. 10 we report the calculated DFT-LDA energy loss function for cubic BN, namely $Im[-1/\epsilon(q, \omega)]$, in comparison with the experiments. We compare our results with Electron Energy Loss (EEL) measurements of McKenzie et al. [43]. The dominant maximum in the EEL spectrum is due to the plasmon excitation, a longitudinal oscillation of the valence electrons as a whole against the cores, classically occurring at frequency $\omega_p^2 = Ne^2/m$ where N represents the density of the valence electrons of the sample. Due to the different density of h-BN and c-BN, EEL spectra have been used to discriminate between the two phases within the same specimen [43]. The measured ω_p for h-BN is 25.5eV and for the c-BN is 28.5eV . An absorption threshold for the cubic phase at 9eV has been deduced by the authors of ref. [43]. Our DFT-LDA calculation yields a first peak at 30eV , which is in reasonable agreement with the experimental one (28.5 eV) and with that determined by Xu and Ching (28eV) [24].

V. LAYERED HEXAGONAL BN

For this material conflicting experimental and theoretical values of the fundamental band gap can be found in the literature. Tarrío e Schatterly presented EELS spectra between $0 \div 60$ eV, with a plasmon peak at 26.4eV. From their data, a direct gap of 5.9 ± 0.2 eV was inferred [47]. Catellani and coworkers using a linear augmented plan wave computational scheme (FLAPW-LDA), claimed that h-BN has a minimal indirect gap at the $H_{3v} - M_{1c}$ transition, corresponding to 3.9 eV, and a minimal direct gap at 4.3 eV, corresponding to the $H_{3v} - H_{2c}$ transition [31]. Hoffman and coworkers, by optical reflectivity measurements in the range $0.045 \div 10$ eV, found a direct gap of 5.2 ± 0.2 eV, deducing that it correspond to direct transitions at H [48]. Park, Terakura, Hamada, using a FLAPW (LDA) scheme, found a minimal direct gap, and gave for the $M_v - M_c$ transition energy a value of 4.5 eV [30]. Last but not least, the work of Suhr and coworkers and [33] of Cappellini et al. found, within DFT-GW, that the material has an indirect minimal gap (see section III). For h-BN we start the discussion from the EEL function reported in Fig.11. In this figure, we compare the calculated DFT-LDA curve, averaged over the three crystallographics axis, with the curve calculated by Xu and Ching [24], and with the experimental one by McKenzie [43]. We recognize three major structures. In the theoretical spectrum of ref. [24], a first peak(A) around 7eV can be found, a second peak (B) is at 12eV , and a major structure (C) appears at 24 eV. The latter is the bulk plasmon peak, to be compared with the experimental value of 25.5 eV [43]. In Fig. 12 we report the calculated imaginary part of the dielectric function for x-y and z components. Our results compare well also in this case with the LCAO ones by Xu and Ching. In Fig. 13 we plot the imaginary part of the dielectric function averaged over the three crystallographics axis. In particular after Fig. 12 and Fig. 13, we agree with the conclusions of Xu and Ching that peak B in the EEL function of Fig.11, comes from the component of ϵ_2 parallel to the c axis of the hexagonal crystal, while peak A comes form the perpendicular components of ϵ_2 . These statements may be easily confirmed by considering experimental curves at different scattering momentum transfer (in plane versus

c-axis data) [24,47]. The major peak C contains contributions from both the ϵ_2 components perpendicular and parallel to the c-axis. In Fig. 14 we report the imaginary and real part of the calculated refractive index. Again, a qualitative difference with respect with the cubic case is observable. Infact, although the imaginary part of the dielectric function has been averaged over the three crystallographics directions, strong differences arises with respect to the cubic case (see Fig.(8)).

The knowledge of the optical properties of h-BN can help us to understand the mismatch between theory and experiments for the ϵ_2 of c-BN. Infact, as it was recently shown [74], c-BN films display an hexagonal-like top layer, and in presence of disturbances the amount of disorder in both types of films increases significantly, leading to the transformation of the cubic phase to the hexagonal-like material. Moreover, it has been demonstrated that due to the large hysteresis of the hexagonal-cubic phase transitions, h-BN domains may continue to exist in c-BN sample [15]. It can hence be argued that the experimental samples of c-BN are likely to contain impurities due to h-BN domains. Assuming that the sample used in the experimental work by Osaka and coworkers [46] contained h-BN domains, we can work within the effective crystal approximation, i.e. assuming that the domains are homogeneous and isotropic: in this case an imaginary dielectric function corresponding to a linear combination of the two pure forms can be expected for the merged system [75]:

$$\epsilon_2(\omega) = x\epsilon_2^{h-BN}(\omega) + (1 - x)\epsilon_2^{c-BN}(\omega) \quad (11)$$

with x going from 0 to 0.5. In Fig. 15 we report the results obtained within this scheme always at the DFT-LDA level. By increasing the concentration of h-phase, a peak at 5 eV due to h-BN presence does grow, while the peak (for which the cubic phase is responsible) around 12eV, due to the cubic phase decreases. Even if the main peak comes in better agreement with the experiments in intensity, the peak around 5eV remains significantly red shifted with respect with the experimental onset. To address more deeply this issue, we calculate self-energy corrections to the spectra of both phases within the GW approximation [25]. The results are reported in Fig. 16. The GW corrected spectrum matches the experimental

threshold better than the DFT-LDA one, but the major peak now misses completely the main experimental structure at 11.7eV.

Another possible explanation to the mismatch between theory and experiment for the cubic phase is the contribution of higher-order effects in the spectra, like those due to the electron-hole interaction which we have neglected so far. If we consider, in Fig. 16, the case with $x=0$ (pure c-BN with GW self-energy corrections), the GW theoretical onset falls at 11.6eV (see section 1), more than 5eV higher than the experimental one ($\sim 5.8eV$ by Osaka). Hence the inclusion of self-energy effects in the DFT-LDA spectrum worsens the comparison with experiments in the present case. An effect of this type is typical for systems where the excitonic effects are large. The excitonic binding energies in fact, can range from few meV (like in bulk GaAs and Si) to much larger values (of the order of the eV) in insulating oxides [76,77,78]. The effects of self-energy and excitonic corrections to the DFT-LDA ϵ_2 curve roughly correspond to shifts in opposite directions [76,78]. Referring to the onset of ϵ_2 , one might obtain a rough estimate of the excitonic binding energy from the mismatch between GW corrected onset and the experimental one. In the c-BN case, a value of more than 5eV would occur. This value seems to be too high, even in comparison with the strongest exciton binding energies found in systems like oxides, where, due to the weak screening, the electron and the hole can be bound by an energy binding of the order of 1eV [76]. A theoretical evaluation based on Wannier functions for c-BN leads to a value of this order of magnitude [88]. To fully address this problem from the theoretical point of view, one should solve the Bethe-Salpeter equation for the optical response function including two particle effects [76,77,78]. On the other hand, one should look for more refined experimental measurements of the linear optical properties of c-BN. In summary c-BN and h-BN mixing within the sample, self-energy and excitonic effects, the presence of impurities, the lack of pure crystalline samples, and lattice parameter mismatch, can in principle all be sources of the disagreement between theoretical results and the available spectra for c-BN.

VI. CONCLUSIONS

Linear optical functions of cubic and hexagonal BN have been studied within DFT-LDA. Calculated energy-loss functions compare well with experiments and with previous theoretical results, both for h-BN and c-BN. Discrepancies arise between theoretical results and experiments in the imaginary part of the dielectric function for c-BN. Possible explanations to this issue are proposed and evaluated; lattice constant variations, h-BN contamination in c-BN samples, and self-energy effects. On the other hand our DFT-LDA results show a reasonable agreement with other theoretical outcomes and with experiments for the imaginary part of the dielectric function in the case of h-BN. More refined measurements and calculations are needed to fully address the mismatch between theory and experiment for the cubic case. It is in our programs to go further in direction of a refinement of the calculations.

VII. ACKNOWLEDGEMENTS

We thank R. Del Sole, P. Monachesi, G. Adragna, and A. Marini for useful discussions. We acknowledge the help of G. Pusceddu for generating pseudopotentials used in this work.

REFERENCES

- [1] L. Kleinmann, J.C. Phillips, Phys. Rev. **117**, 460 (1960)
- [2] E.Doni, G.Pastori Parravicini, Nuovo Cimento **64B**, 117 (1969)
- [3] H.R. Philipp, E.A. Taft, Phys. Rev. **127**, 159 (1962)
- [4] J.H. Edgar, *Properties of Group III Nitrides*, Ed. by J.H. Edgar, Kansas State University (U.S.A.), INSPEC, Institution of Electric Engineers, 7 (1994)
- [5] T.K. Pauli, P. Bhattacharya, D.N. Bose, Appl. Phys. Lett. **56**, 2648 (1990)
- [6] S.S. Dana, Mater. Sci. Forum **54-55**, 229 (1990)
- [7] K. Miyoshi, D.H. Buckley, J.J. Pouch, S.A. Alterovitz, H.E. Sliney, Surf. Coat. Technol. **33**, 221 (1987)
- [8] X. Blase, A.Rubio, S.G. Louie, M.L. Cohen, Europhysics Letters (b) **28**, 335 (1994)
- [9] A.Rubio, J.L. Corkill, M.L. Cohen, Phys. Rev. B **49**, 5081 (1994)
- [10] X. Blase, A.Rubio, S.G. Louie, M.L. Cohen, Phys. Rev. B **51**, 6868 (1995)
- [11] L. Vel, G. Demazeau, J. Etourneau, J.J. Pouch, Mat. Sci. Eng. B **10**, 149 (1991)
- [12] M.J. Powers, M.C. Benjamin, L.M. Porter, R.J. Nemanich, R.F. Davis, J.J. Cuomo, G.L. Doll, S.J. Harris, Appl. Phys. Lett. **65**, 3912 (1995)
- [13] R.W. Pryor, Appl. Phys. Lett. (68), 13 (1996)
- [14] B.F. Williams, R.E. Simon, Appl. Phys. Lett. **14**, 214 (1969)
- [15] M.I. Eremets, K. Takemura, H. Yusa, D. Goldberg, Y. Bando, V.D. Blank, Y. Sato, K. Watanabe, Phys. Rev. B **57**, 5655 (1998)
- [16] V.L. Solozhenko, J. Hard Mater. **6**, 51 (1995)
- [17] V.L. Solozhenko, *Properties of Group III Nitrides*, Ed. by J.H. Edgar, Kansas State Uni-

versity (U.S.A.), INSPEC, Institution of Electric Engineers, 7 (1994)

- [18] G. Kern, G. Kresse, J. Hafner Phys. Rev. B **59**, 8551 (1999)
- [19] M. Sokolowski, J. Cryst. Growth **46**, 136 (1979)
- [20] J. Furthmüller, J. Hefner, G. Kresse, Phys. Rev. B **50**, 15606 (1994)
- [21] K. Albe, Phys. Rev. B **55**, 6203 (1997)
- [22] R.M. Wentzcovitch, K.J. Chang, M.L. Cohen, Phys. Rev. B **34**, 1071 (1986)
- [23] R.M. Wentzcovitch, S. Fahy, M.L. Cohen, S.G. Louie, Phys. Rev. B **38**, 6191 (1988)
- [24] Y.-N. Xu, W.Y. Ching, Phys. Rev. B **44**, 7787 (1991)
- [25] G. Cappellini, V. Fiorentini, K. Tenelsen, F. Bechstedt Mat. Res. Soc. Symp. Proc. (b) **395**, 429 (1996)
- [26] A. Zunger, A. Katzir, A. Halperin, Phys. Rev. B **13**, 5560 (1976)
- [27] Y.F. Tsay, A. Vaidyanathan, S.S. Mitra, Phys. Rev. **19**, 5422 (1979)
- [28] R. Dovesi, C. Pisani, C. Roetti, P. Dellarole, Phys. Rev. **24**, 4170 (1981)
- [29] J. Robertson, Phys. Rev. **29**, 2131 (1984)
- [30] K. T. Park, K. Terakura, N. Hamada, J. Phys. C: Solid State Phys. **20**, 1241-1251 (1987)
- [31] A. Catellani, M. Posternak, A. Baldereschi, A.J. Freeman, Phys. Rev. B **36**, 6105 (1987)
- [32] P.E. Van Camp, V.E. Van Doren, J.T. Devreese, Solid State Comm. **71**, 1055 (1989)
- [33] M. P. Suhr, S. G. Louie, M.L. Cohen, Phys. Rev. B **43**, 9126 (1991)
- [34] Y.-N. Xu, W.Y. Ching, Phys. Rev. B **48**, 4335 (1993)
- [35] N. E. Christensen, I. Gorczyca, Phys. Rev. B **50**, 4397 (1994)
- [36] V. I. Gavrilenko, R.Q. Wu, Phys. Rev. B **61**, 2632 (2000)

- [37] G. Cappellini, G. Satta, K. Tenelsen, F. Bechstedt, Phys. Stat. Sol. (b) **95**, 861 (2000)
- [38] R.D. Carson, S.E. Schatterly, Phys. Rev. Lett. **59**, 319 (1987)
- [39] J.J. Jia, T.A. Callcot, E.L. Shirley, J.A. Carlisle, L. J. Terminello, A. Asfaw, D.L. Ederer, F.J. Himpsel, R.C.C. Perera, Phys. Rev. Lett. **76**, 4054 (1996)
- [40] C. Oshima, A. Nagashima, J. Phys. : Condens. Matter **9**,1 (1997)
- [41] B.M. Davies, F. Bassani, F.C. Brown, Phys. Rev. **B24**, 3537 (1981)
- [42] I. Jimenez, A.F. Jankowski, L.J. Terminello, J.A. Carlisle, D.G.J. Sutherland, G. L. Doll, J. V. Mantese, W. M. Tong, D. K. Shuh, F.J. Himpsel, Phys. Rev. B **55**, 12025 (1997)
- [43] D.R. McKenzie, W.G. Saintry, D. Green, *Materials Science Forum*, Vol. **54-55**, pp.193-206(1990)
- [44] U. Büchner, Phys. Stat. Sol. (b) **81**, 227 (1977)
- [45] N. Miyata, K. Moriki, O. Mishima, M. Fujisawa, T. Hattori Phys. Rev. B **40**, 12028 (1989)
- [46] Y. Osaka, A. Chayahara, H. Yokohama, M. Okamoto, T. Hamada, T. Imura, M. Fujisawa , *Synthesis and Properties of Boron Nitride*, edited by J.J. Pouch and S.A. Alteroviz , Vol. **54 & 55**, Trans Tech, Aedermannsdorf, Switzerland, 1990,pp.277-294
- [47] C. Tarrío, S.E. Schatterly, Phys. Rev. B **40**, 7852 (1989)
- [48] D.M. Hoffman, G. L. Doll, and P.C. Eklund, Phys. Rev. B **30**, 6051 (1984)
- [49] R.M. Chrenko, Solid State Comm. **14**, 511-515 (1974)
- [50] R.M. Dreizel, E.K.U. Gross, *Density Functional Theory*, Springer, N.Y., 1990
- [51] D. M. Ceperley and B. J. Alder, Phys. Rev. Lett. **45**, 566 (1980)
- [52] J.P. Perdew, A. Zunger, Phys. Rev. B **23**, 5048 (1981)
- [53] X. Gonze, R. Stumpf and M. Scheffler, Phys. Rev. B **44**, 8503 (1991)

- [54] M. Fuchs, M. Scheffler, *Computer Physics Communications* **119**, 67 (1999)
- [55] N. Troullier and J. L. Martins, *Phys. Rev. B* **43**, 1993 (1991)
- [56] S.G. Louie, S. Froyen, M.L. Cohen, *Phys. Rev. B* **26**, 1738 (1982)
- [57] D.J. Chadi, M.L. Cohen, *Phys. Rev.* **8**, 5747 (1973)
- [58] C.R. Aita, *Synthesis and Properties of Boron Nitride*, edited by J.J. Pouch and S.A. Alteroviz , Vol. **54** & **55**, Trans Tech, Aedermannsdorf, Switzerland, 1990, pp. 1-20
- [59] O. Pulci, G. Onida, A.I. Shkrebtii, R. Del Sole, B. Adolph, *Phys. Rev.* **55**, 6685 (1997)
- [60] B. Adolph, V.I. Gavrilenko, K. Tenelsen, F. Bechstedt, R. Del Sole *Phys. Rev.* **53**, 9797 (1996)
- [61] F. Bassani, G. Pastori Parravicini, *Electronic States and Optical Tansitions in Solids*, Pergamon Press, Oxford, (1973); A. Baldereschi, A. Quattropani, *Theorie Electronique du Solide*, EPFL Lecture Notes, Lausanne 1985
- [62] M.S. Hybertsen and S.G. Louie, *Phys. Rev. B* **34**, 5390 (1986)
- [63] F. Bechstedt, *Festkörperprobleme-Advances in Solid State Physics*, **32**, ed. by U Rössler (Vieweg, Braunschweig/Wiesbaden, 1992), p.161
- [64] F. Bechstedt, R. Del Sole, *Phys. Rev. B* **38**, 7710 (1988)
- [65] F. Gygi, A. Baldereschi, *Phys. Rev. Lett.* **62**, 2160 (1989)
- [66] L. Hedin, *Phys. Rev.* **139**, A796 (1965); L. Hedin and S. Lundqvist, *Solid State Phys.* **23**, 1 (1969)
- [67] R. Godby, M. Schlüter and L. J. Sham, *Phys. Rev. B* **37**, 10159 (1988)
- [68] F. Bechstedt, R. Del Sole, G. Cappellini, L. Reining, *Solid State Comm.* **84**, No. 7, pp.765-770, 1992

- [69] M. Palummo, R. Del Sole, Lucia Reining, F. Bechstedt, G. Cappellini, Solid State Comm. **95** N.6, 393-398 (1995); B. Wenzien, G. Cappellini, F. Bechstedt, Phys. Rev. B **51**, 14701 (1995); B. Wenzien, P. Käckell, F. Bechstedt, G. Cappellini, Phys. Rev. B **52**, 10897 (1995)
- [70] X. Blase, A. Rubio, S.G. Louie, M.L. Cohen, Phys. Rev. B **51**, 6868 (1995);
- [71] O. Madelung, *Semiconductor Basic Data*, Springer, Berlin (1996)
- [72] P. Monachesi, private communication
- [73] M. Palummo, L. Reining, R. W. Godby, C.M. Bertoni, N. Borsari, Europhys Lett. **26**, 607 (1994)
- [74] P. Widmayer, H.-G. Boyen, P. Ziemann, P. Reinke, P. Oelhafen, Phys. Rev. B **59**, 5233 (1999)
- [75] V. Fiorentini, A. Baldereschi, J. Phys. : Condens. Matter **4**, 5967 (1992) and references therein
- [76] S. Albrecht, G. Onida, L. Reining, Phys. Rev. B **55**, 10278 (1997)
- [77] S. Albrecht, L. Reining, R. Del Sole, G. Onida, Phys. Stat. Sol. (a) **170**, 189 (1998)
- [78] M. Rohlfing, S.G. Louie, Phys. Rev. Lett. **81**, 2312 (1998)
- [79] R.M. Wentzcovitch, M.L. Cohen, P.K. Lam, Phys. Rev. B **36**, 6058 (1987)
- [80] W. Sekkal, B. Bouhafs, H. Aourag, M. Certier, J. Phys. C: Solid State Phys. **10**, 4975-4984 (1998)
- [81] R. Pandey, J. E. Jaffe, and A. B. Kunz, Phys. Rev. B **43**, 9228 (1991)
- [82] P. Fulde, *Electron Correlations in Molecules and Solids*, Springer-Verlag, Berlin (1991).
- [83] W. Kohn and L.J. Sham, Phys. Rev **140**, A1133 (1965)

- [84] M.S.Hybertsen and S.G.Louie, Phys. Rev. B **37**, 2733 (1988)
- [85] G. Cappellini, S. Bouette-Russo, B. Amadon, C. Noguera, F. Finocchi, J. Phys. : Condes. Matter **12**, 3671-3688 (2000)
- [86] L.Reining, G. Onida, R. W. Godby, Phys. Rev. B **56**, 4301 (1997)
- [87] Gielisser, PR **155**, 1039 (1967)
- [88] G. Adragna, Master Degree Thesis , II University of Rome,1998 and private communication
- [89] Z.H. Levine, S.G. Louie, Phys.Rev. B **25**, 6310 (1982)
- [90] G. Cappellini, R. Del Sole, L. Reining, F. Bechstedt, Phys. Rev. B **47**, 9892 (1993)
- [91] S.J. Jenkins, G.P. Srivastava, J.C. Inkson Phys. Rev. B **48**, 4388 (1993)
- [92] F. Gygi, A. Baldereschi, Phys. Rev. B **34**, 4405 (1986)
- [93] A. Hasegawa and A. Yanase, J. Phys. C **13**, 1995 (1980)
- [94] K. J. Chang and M. L. Cohen, Phys. Rev. B **30**, 4774 (1984)
- [95] U. Schöemberger and F. Aryasetiawan, Phys. Rev. B **52**, 8788 (1995)
- [96] O. E. Taurian, M. Springborg and N. E. Christensen, Solid State Comm. **55**, 351 (1985)
- [97] P. Cortona and A. Villaflorita Monteleone, J. Phys. Cond. Matt. **8**, 8983 (1996)
- [98] V. Fiorentini, Phys. Rev. B **46**, 2086 (1992)
- [99] K. Karch, F. Bechstedt, Phys. Rev. B **56**, 7404 (1997)

TABLES

c-BN	Work1	Work2	Theo1	Theo2	Exp.
$a_0(a.u.)$	6.754	6.771	6.759	6.833	6.833
$B_o(Mbar)$	4.01	3.52	3.97	3.70	3.69-4.65
$h - BN$					
$a_0(a.u.)$	4.698	4.68	4.50	4.71	4.72
c/a	2.608	2.6068	2.608	2.670	2.664
$B_o(Mbar)$	2.68	2.65	2.61	3.35	

TABLE I. Calculated structural properties of zincblende and hexagonal BN (lattice constant and bulk modulus) compared with other theoretical and experimental results. First column: present calculations; second column: theoretical results by Cappellini et. al. [25], Theo1: results by Furthmüller et al. [20], Theo2: results by Xu e Ching [24], and in the last column the experimental values from Ref. [25].

c-BN	GW1	GW1bis	GWf	Exp
$\Gamma_{15'v} - X_{1c}$	7.28	6.95	6.3	6.4 ± 0.5
$\Gamma_{15'v} - \Gamma_{1c}$	11.79	11.46	11.4	14.5

TABLE II. Excitation energies for c-BN. In the first column, the present theoretical values here calculated (GW1), GW1bis is taken from Ref. [25], GWf from Ref. [33]. The experimental results for the indirect gap are from Ref. [49], and those for the direct one are from Ref. [3].

h-BN	GW1	GW1bis	GWf	Exp
$H_{3v} - M_{1c}$	6.39	6.04	5.4 ^a	5.2 ± 0.2
$H_{3v} - H_{2c}$	6.76	6.66	6.33 ^b	

TABLE III. Excitation energies for h-BN . The first column contains the values calculated here (GW1), GW1bis is taken from Ref. [25], GWf from Ref. [10] and the experimental values from Ref. [48]. For the meaning of the a and b marks, see text.

FIGURES

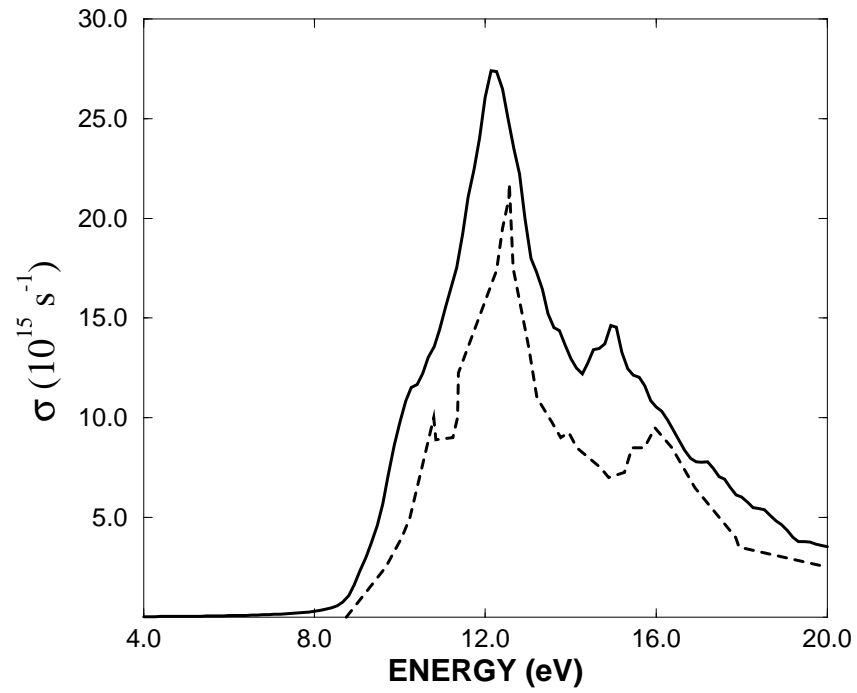


FIG. 1. Calculated optical conductivity σ of c-BN (solid line) vs. the theoretical result of Ref. [24] (dashed line).

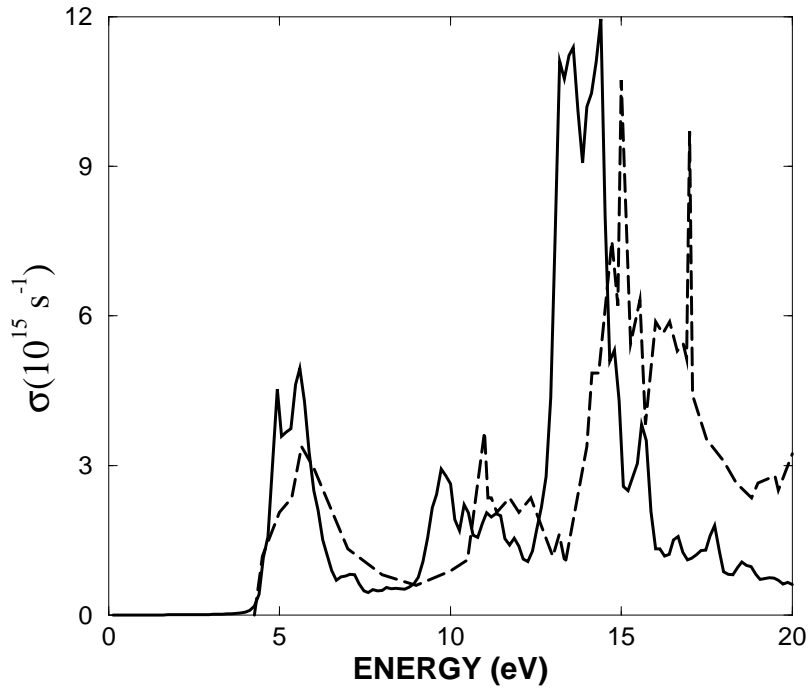


FIG. 2. Optical conductivity function of h-BN (solid line) vs. previous theoretical result (dashed line) after Ref. [24].

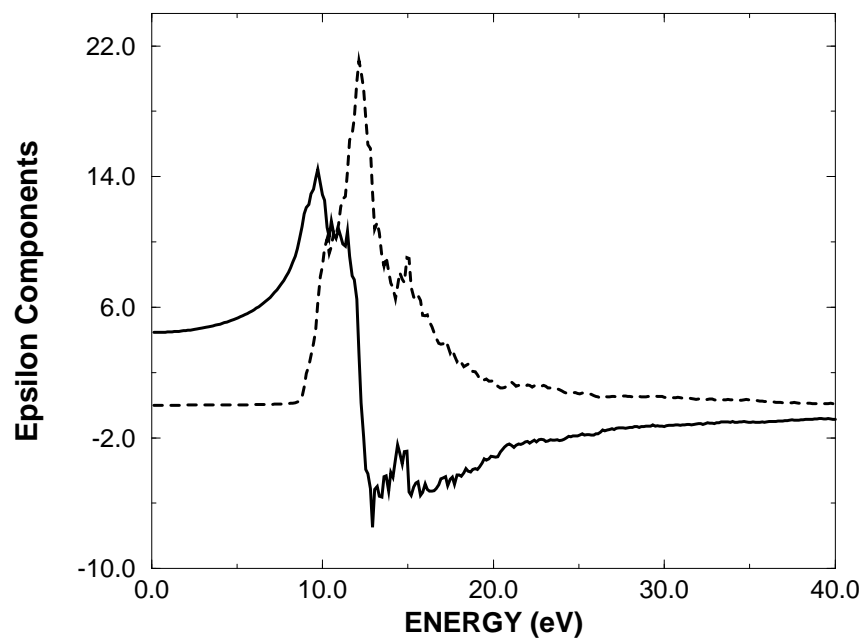


FIG. 3. Computed real and imaginary parts of the dielectric function for c-BN. ϵ_1 is the solid line, ϵ_2 the dashed one.

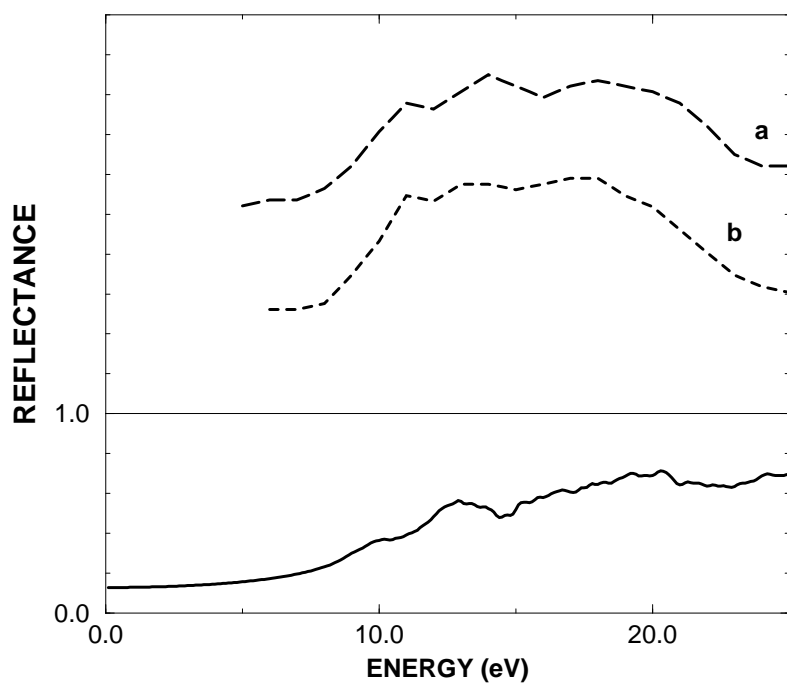


FIG. 4. Calculated reflectivity (solid line) of c-BN vs. experimental results in arbitrary units (dashed lines), taken from Ref. [46].

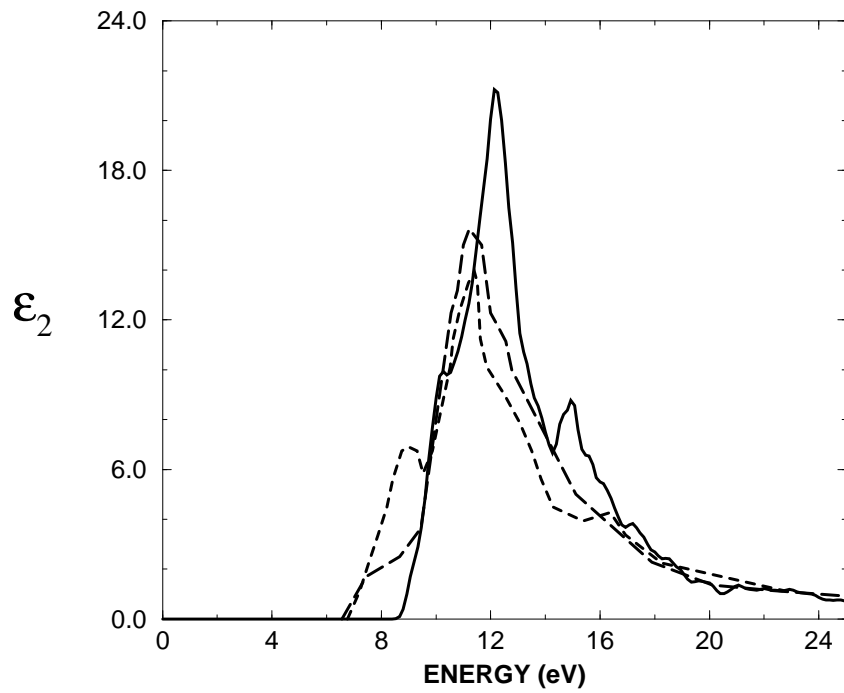


FIG. 5. Calculated imaginary part of dielectric function of c-BN (solid line) vs. the experimental results of Ref. [46] (dashed lines).

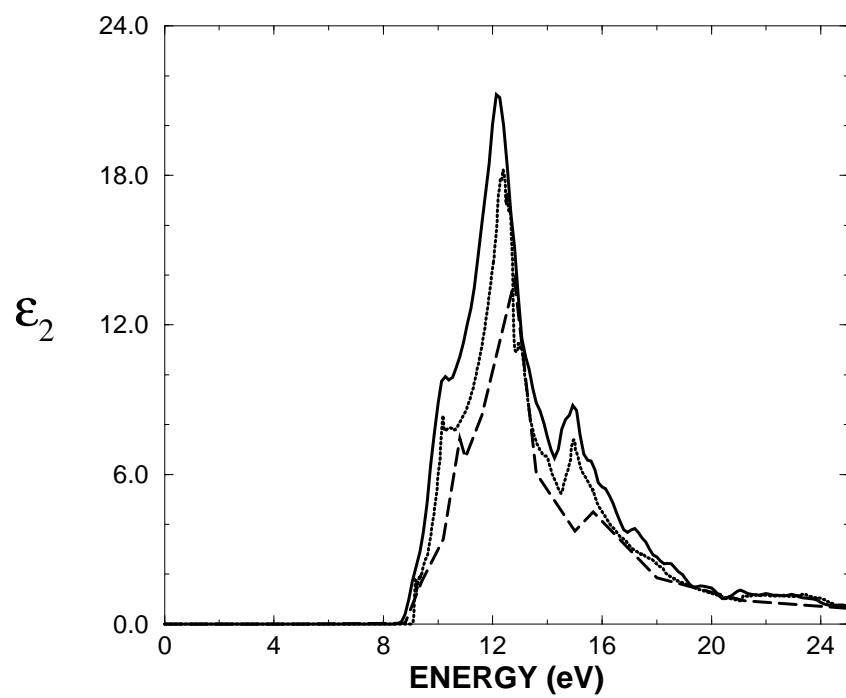


FIG. 6. Calculated imaginary part of dielectric function of c-BN (solid line) vs. LMTO result after Ref. [72] (dotted line) and LCAO result (dashed line) of Ref. [24].

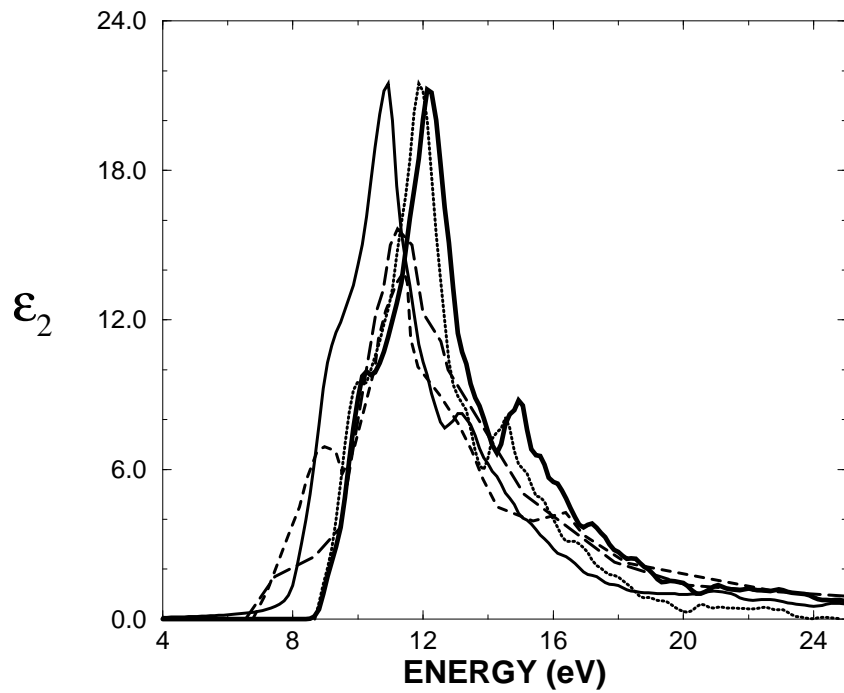


FIG. 7. Calculated imaginary part of dielectric function of c-BN at experimental (dotted line) , theoretical (bold solid line) and theoretical plus 5% (solid line) lattice constant. Experimental results (dashed lines) after Ref. [46] are plotted for reference.

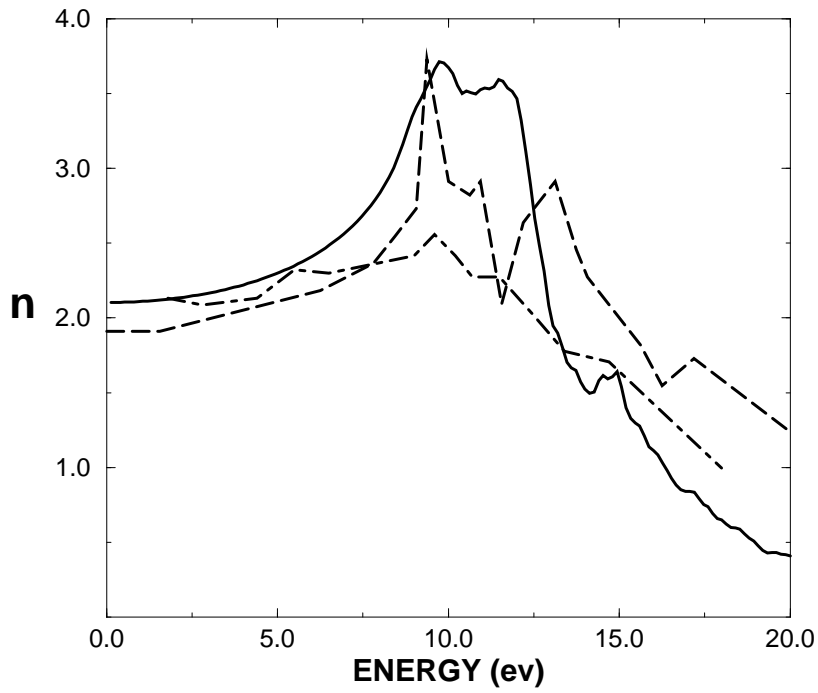


FIG. 8. Calculated real part of refractive index of c-BN (solid line) vs. the experimental results (dot-dashed line after Ref. [45]) , and previous theoretical result (dashed line after Ref. [24]).

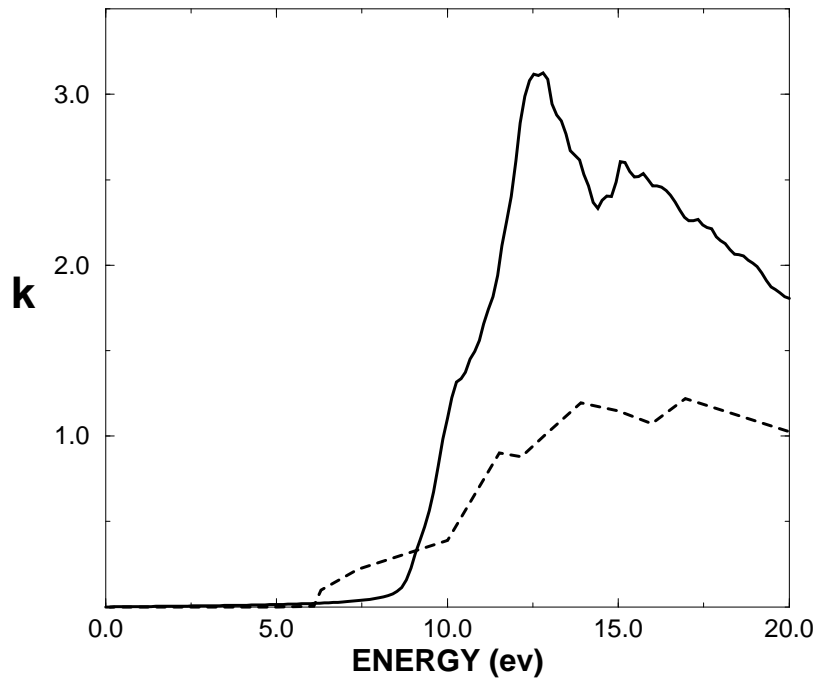


FIG. 9. Calculated imaginary part of refractive index of c-BN (solid line) vs. experimental results (dashed line) after Ref. [45].

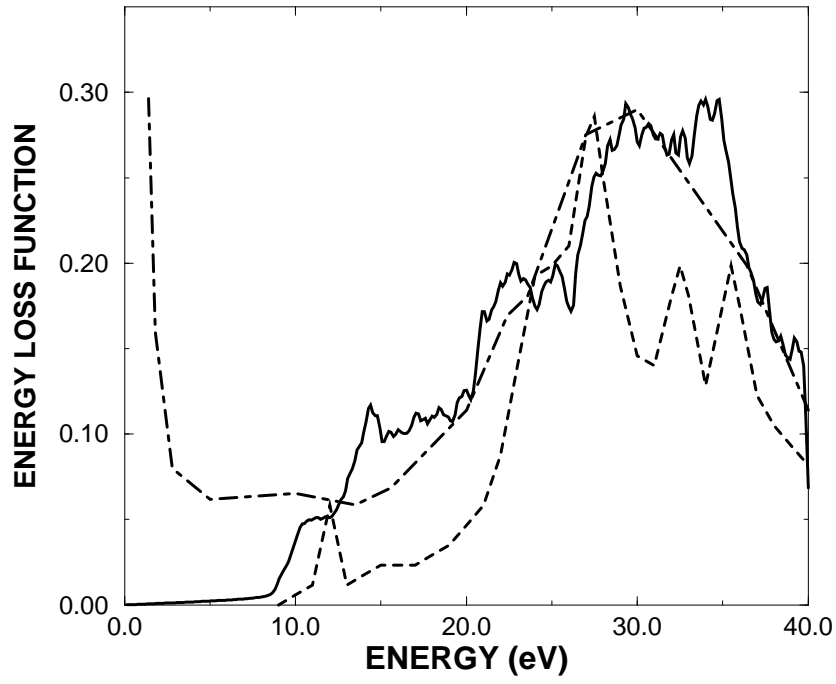


FIG. 10. Energy-loss function of c-BN (solid line) vs. the experimental result (dot-dashed line) after Ref. [43] and previous theoretical result (dashed line) of Ref. [24].

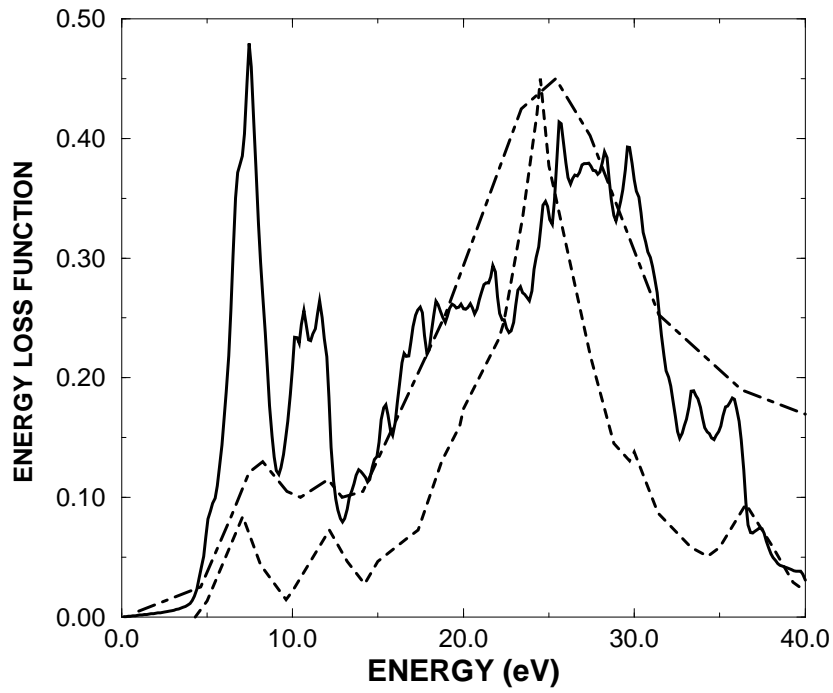


FIG. 11. Energy-loss function of h-BN (solid line) vs. the experimental result (dot-dashed line) of Ref. [43] and previous theoretical result (dashed line) after Ref. [24].

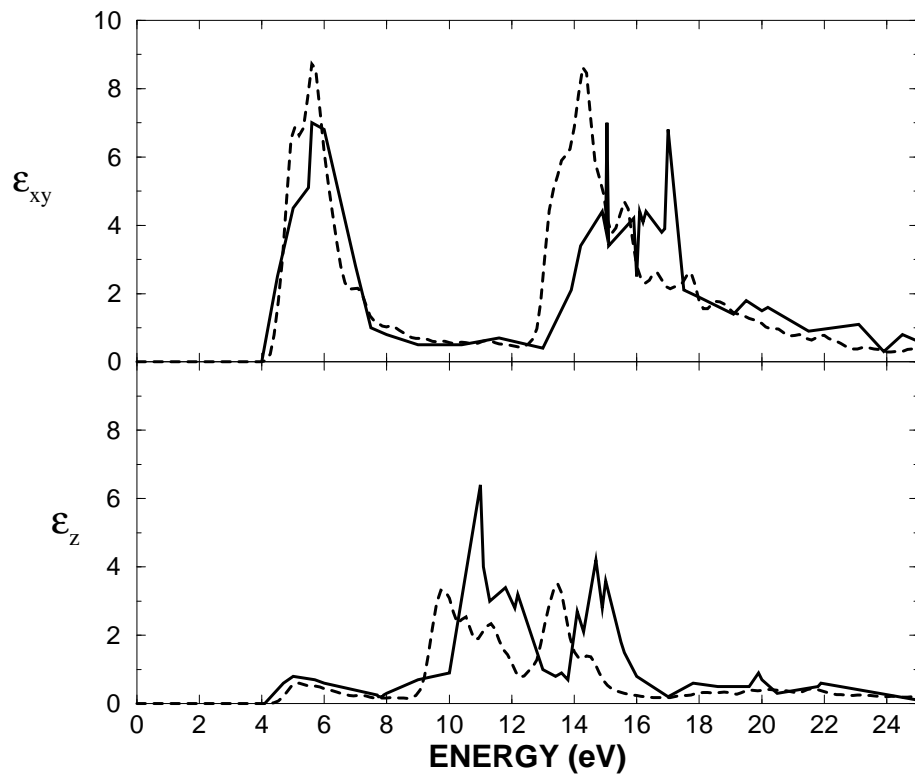


FIG. 12. First panel: imaginary part of the dielectric function of h-BN (solid line) averaged on x and y directions vs. the same quantity after Ref. [24] (dashed line). Second panel: imaginary part of the dielectric function of h-BN (solid line) on z direction vs. the same quantity after Ref. [24] (dashed line).

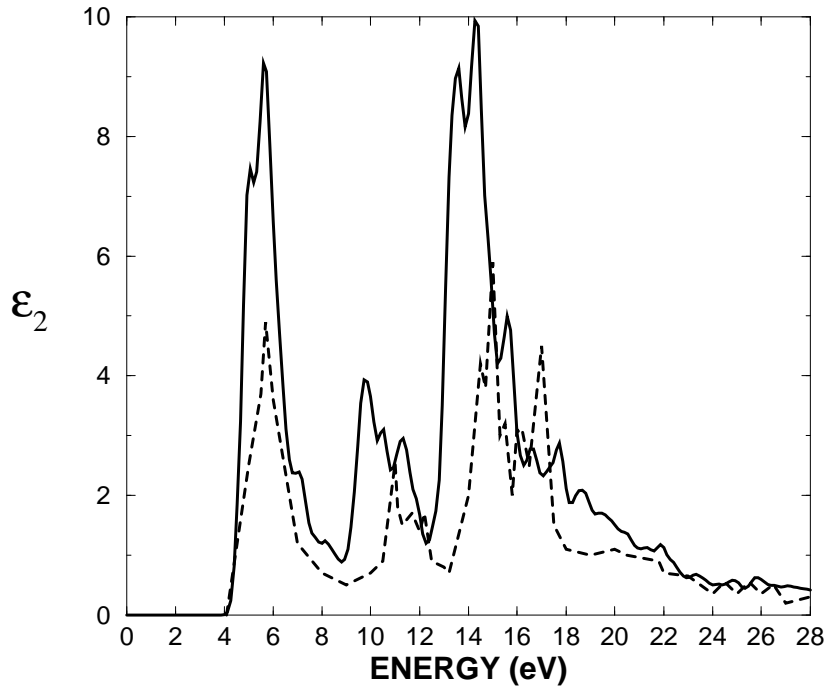


FIG. 13. Imaginary part of dielectric function of h-BN (solid line) vs. previous theoretical result of Ref. [24] (dashed line) averaged over the three crystallographic directions.

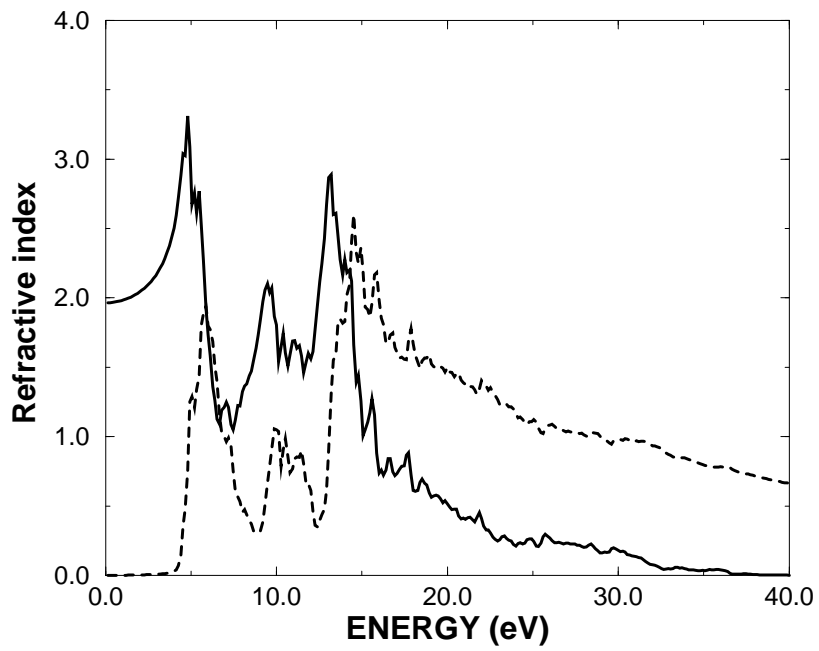


FIG. 14. Calculated refractive index of h-BN: real (solid line) and imaginary part (dotted line).

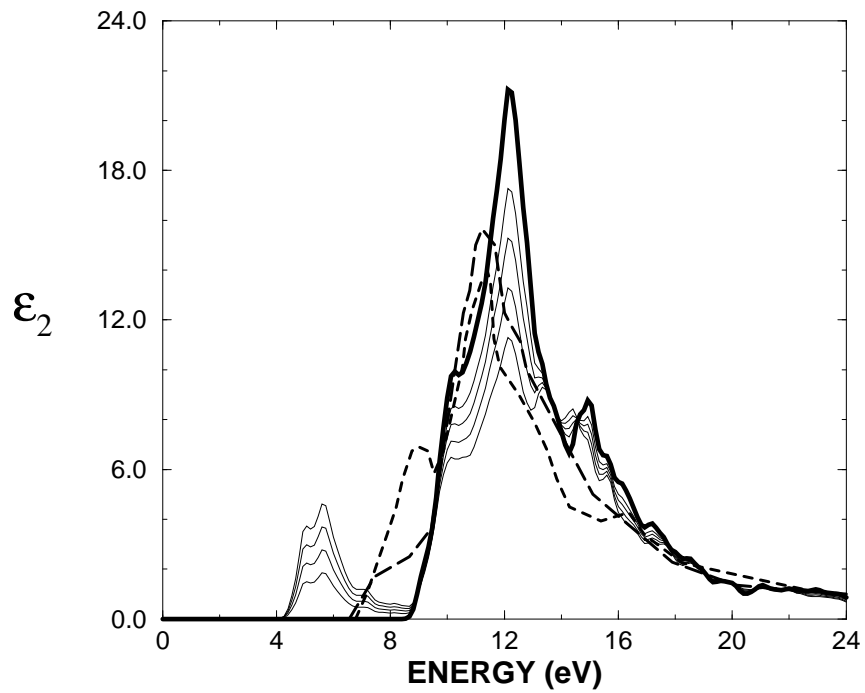


FIG. 15. Imaginary part of dielectric function for merged c-BN and h-BN (solid lines). The experimental results of Ref. [46] are also given (dashed lines). Pure cubic ϵ_2 is showed with bold solid line.

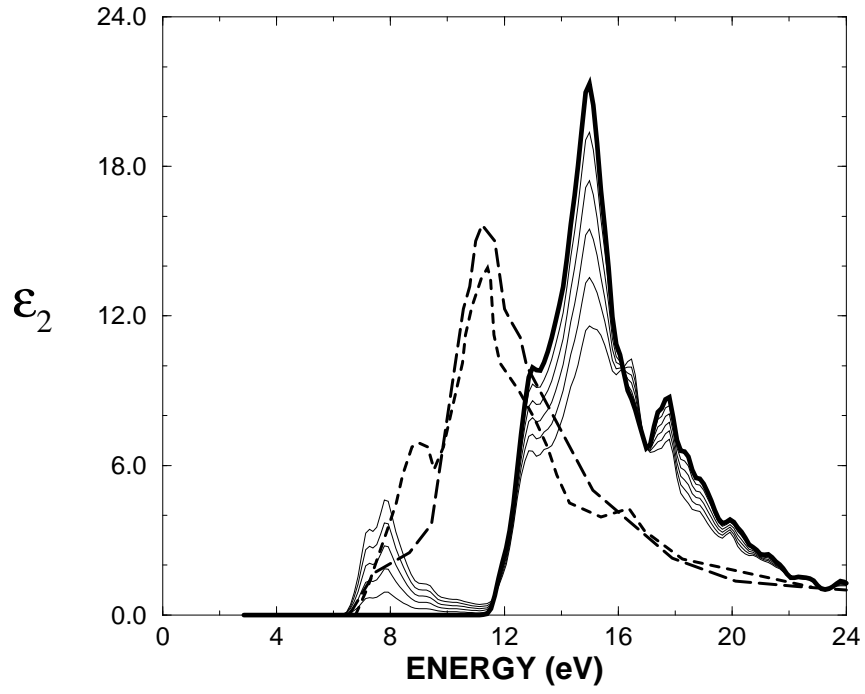


FIG. 16. Imaginary part of dielectric function with GW corrections (see text) for merged c-BN and h-BN (solid lines). Experimental results of Ref. [46] are also given (dashed lines). Pure cubic ϵ_2 is showed with bold solid line.